

Block-Copolymer-Based Plasmonic Nanostructures

Peter A. Mistark,[†] Soojin Park,^{*,§,*} Sibel Ebru Yalcin,[†] Dong Hyun Lee,[§] Ozgur Yavuzcetin,[†] Mark T. Tuominen,[†] Thomas P. Russell,[§] and Marc Achermann^{†,*}

[†]Physics Department, University of Massachusetts, Amherst, Massachusetts 01003, [§]School of Energy Engineering, Ulsan National Institute of Science and Technology, Ulsan, 689-798 Korea, and [§]Department of Polymer Science and Engineering, University of Massachusetts, Amherst, Massachusetts 01003

Metal nanostructures are basic building blocks for metamaterials and plasmonic circuits and sensors. They give rise to the unusual optical properties of metamaterials, such as negative refractive indices,¹ perfect focusing,² or hyperbolic dispersion relations.³ On the other hand, surface plasmon (SP) excitations in nanoscale metal structures lead to the functionality of plasmonic circuits and sensors that allow for smaller and more sensitive photonic devices.⁴ To operate at visible or near-infrared frequencies, both material categories rely on specifically designed metal structures with nanoscale dimensions. Interference lithography has shown to be an attractive technique for producing such nanostructures in large arrays with typical sizes and pitches on the order of 100 nm.⁵ If smaller nanostructures in denser arrays are required, high-resolution electron beam or focused ion beam lithography is often chosen. Since these lithography techniques are not well-suited for large areas, alternative strategies are required. Self-assembly techniques are attractive because they are highly parallel in nature and enable large-scale patterning rapidly and at very low costs. Various self-assembly techniques have been used to produce metal nanostructures and assemblies including nanosphere lithography,⁶ drop deposition,⁷ and DNA-based processes.⁸

The self-assembly of block copolymers (BCPs) can be used to produce highly ordered nanostructures over large surface areas^{9–12} and to generate metal nanoparticles^{13–15} and structured metal surfaces.^{16,17} Here, we use BCP templates to fabricate large arrays of highly ordered gold and gold/silver composite nanoparticles. These arrays show characteristic local surface plasmon (LSP) resonances and, when

ABSTRACT We report on the fabrication and optical characterization of dense and ordered arrays of metal nanoparticles. The metal arrays are produced by reducing metal salts in block copolymer (BCP) templates made by solvent annealing of poly(styrene-*b*-4-vinylpyridine) (PS-*b*-P4VP) or poly(styrene-*b*-ethylene oxide) (PS-*b*-PEO) diblock copolymer thin films in mixed solvents. The gold and gold/silver composite nanoparticle arrays show characteristic surface plasmon resonances in the visible wavelength range. The patterning can be applied over large areas onto various substrates. We demonstrate that these metal nanoparticle arrays on metal thin films interact with surface plasmon polaritons (SPPs) that propagate at the film/nanoparticle interface and, therefore, modify the dispersion relation of the SPPs.

KEYWORDS: local surface plasmon · surface plasmon polariton · block copolymer · gold nanoparticle · gold/silver nanoparticle

deposited onto plane silver films, change the propagation properties of surface plasmon polaritons (SPPs). Hence, such metal nanoparticle arrays are promising functional components for plasmonic devices and can serve as substrates for sensor applications or as templates for producing metamaterials with hyperbolic dispersion properties.

RESULTS AND DISCUSSION

For many optical applications, it is desirable to have plasmonic substrates with SP resonances in the visible wavelength range. Small gold nanostructures fulfill this requirement and, in addition, are very inert and robust toward degradation. We fabricated Au nanoparticle arrays using BCP templates that were prepared by spin-coating solutions of PS-*b*-P4VP diblock copolymer in toluene/tetrahydrofuran (THF) solutions onto glass coverslips. Highly ordered cylindrical P4VP microdomains oriented normal to the film surface were obtained by annealing in a saturated THF environment for 3 h.⁹ The solvent-annealed films were then immersed in a gold salt solution for 5 min to complex gold ions with

*Address correspondence to spark@unist.ac.kr, achermann@physics.umass.edu.

Received for review September 17, 2009 and accepted November 16, 2009.

Published online November 30, 2009. 10.1021/nn901245w

© 2009 American Chemical Society

the 4-vinylpyridine units. Oxygen plasma etching or sodium borohydride (NaBH_4) was used to reduce the gold salt into gold nanoparticles. While the reducing agent procedure leaves the polymer template intact and results in embedded Au nanoparticles, the oxygen plasma degrades the polymer template completely; therefore, we used the latter structures for the scanning force microscopy (SFM) analysis. Figure 1 shows SFM images of the solvent-annealed PS-*b*-P4VP film and the highly ordered gold nanoparticle array that was prepared from the PS-*b*-P4VP template. The sizes and center-to-center distances of the cylindrical microdomains in the BCP template were 25 and 43 nm, respectively, as determined by SFM (Figure 1a). The thickness of the BCP thin film is ~ 28 nm as measured by ellipsometry. Figure 1b indicates that the diameters, heights, and center-to-center distances of the gold nanoparticles are ~ 17 , ~ 13 , and ~ 43 nm, respectively. These array dimensions correspond to a nanoparticle density of $6.2 \times 10^{10} \text{ cm}^{-2}$ and an area coverage of 14%.

Extinction measurements of the ordered arrays of gold nanoparticles show that the arrays of Au nanoparticles prepared by the reducing agent exhibit a more pronounced LSP resonance than the oxygen plasma treated ones. The Au nanoparticles embedded within the block polymer template are surrounded by a high dielectric environment that enhances SP effects. The Au nanoparticles prepared by the oxygen plasma treatment are exposed to air. In Figure 1c, we show extinction spectra of the embedded Au nanoparticle array taken at normal and at 70° off-normal incidence with p-polarized light. The LSP resonance wavelengths of 533 and 520 nm at 0 and 70° , respectively, indicate the asymmetry of the oblate gold nanoparticles. At 0° , the SP resonance along the long axis is excited, while the blue-shifted extinction peak at 70° is dominated by the SP resonance along the short axis. To compare our measurements with theoretical calculations, we used a simple model of non-interacting, ellipsoidal gold nanoparticles in a homogeneous dielectric environment. Interactions between neighboring nanoparticles are negligible because the particle separation is significantly larger (~ 3 times) than the particle radius.¹⁸ Since the scattering cross section of such small metal particles is significantly smaller than the absorption cross section, σ_{abs} , we calculate the latter to compare with our extinction measurements.¹⁹

$$\sigma_{\text{abs}} = \frac{2\pi\sqrt{\epsilon_d}}{\lambda} \text{Im} \frac{\epsilon_m - \epsilon_d}{L(\epsilon_m - \epsilon_d) + \epsilon_d} \quad (1)$$

in which V is the particle volume, ϵ_m and ϵ_d are the dielectric functions of the metal nanoparticles and the dielectric environment, respectively, and L is a geometrical parameter.¹⁹ For spherical particles $L = 1/3$, which gives the well-known SP resonance condition $\epsilon_m - 2\epsilon_d$

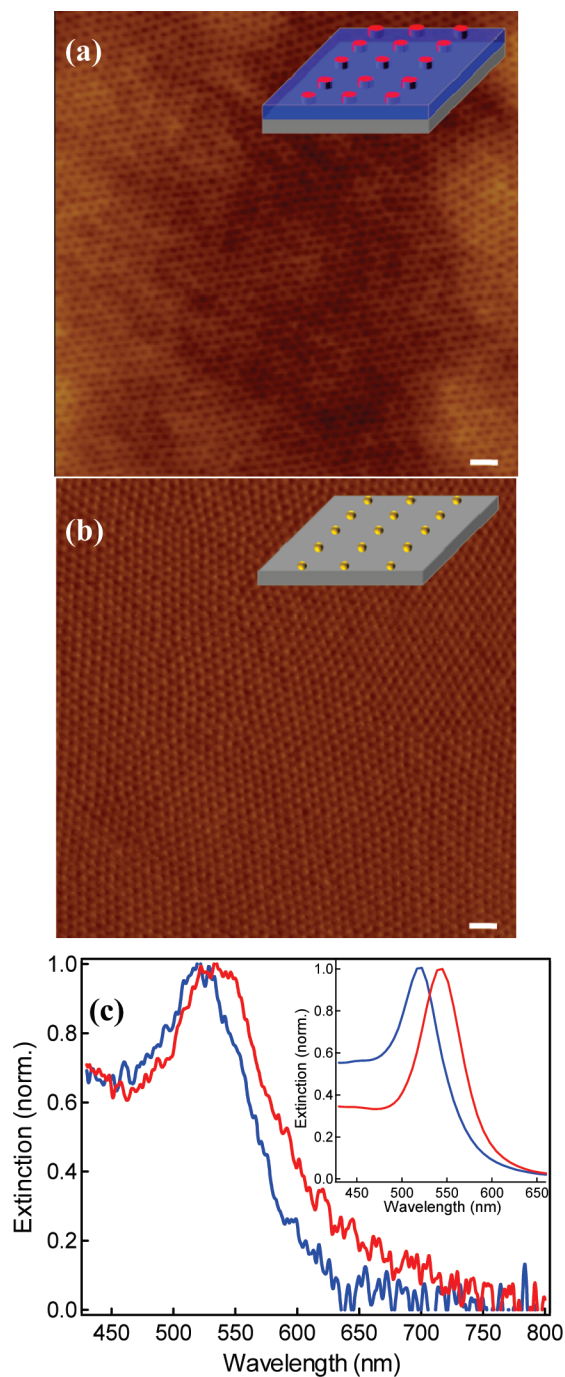


Figure 1. SFM images of the solvent-annealed BCP template (a) and the gold nanoparticle array after removing the BCP template with oxygen plasma treatment (b). Scale bars are 100 nm. Inset in (a): Schematic of the BCP template with the P4VP block in red and the PS block in blue. (c) Extinction spectra of the gold nanoparticle array taken at normal (red) and 70° off-normal incidence (blue). Inset: Calculated absorption spectra of oblate ellipsoids with the electric field polarized along the long axis (red) and the short axis (blue).

$= 0$. On the basis of SFM measurements, we approximate our gold nanoparticles as oblate ellipsoids with short and long half-axes of 6.5 and 8.5 nm, respectively, and obtain L values of 0.41 and 0.3 for electric field polarizations along the short and the long axes, respectively. Such nanoparticles made of gold²⁰ in a dielectric

medium of refractive index 1.5 produce calculated extinction spectra, as shown in the inset of Figure 1c, with LSP resonance wavelengths of 519 and 542 nm for the out- and in-plane SP resonance. Small variations in the input parameters result only in minor changes of the LSP resonance wavelengths.

This simple theoretical model approximates well the measured SP properties of our Au nanoarrays with regard to a longer wavelength in-plane resonance and a shorter wavelength out-of-plane SP resonance. Differences between calculated and measured SP resonance wavelengths are most likely caused by the non-uniform dielectric environment of the gold nanostructures. Another difference is that the measured SP resonance width is ~ 1.6 times broader than the calculated resonance. The broadening of the experimental spectra could be caused by a distribution of nanoparticle sizes that leads to *inhomogeneous* broadening or by surface roughness and crystal defects of the gold nanostructures that lead to additional damping of the SP oscillations and, therefore, an increased *homogeneous* broadening.

The presented synthesis protocol can also be adapted to fabricate multicomponent metal arrays that exhibit two LSP resonances. We achieved this by using BCP templates made of PS-*b*-P2VP/PS-*b*-PEO copolymer blends to produce gold/silver nanoparticle arrays. The purpose of the copolymer blend is that different metal salts can be complexed with different functional groups of the copolymers like vinylpyridine and ethylene oxide. First, a PS-*b*-P2VP/PS-*b*-PEO solution was prepared in toluene and then stirred for 12 h. Toluene is a good solvent for PS, while P2VP and PEO blocks are insoluble in toluene. As-spun BCP thin films form quasi-hexagonal microdomain arrays oriented normal to the film surface, as shown in Figure 2a. We added 0.5 equiv of gold salt (LiAuCl_4) to the polymer solution and stirred for 12 h. LiAuCl_4 incorporates selectively into the PEO block instead of the P2VP block as reported previously.²¹ Subsequently, 0.5 equiv of silver salt (AgNO_3) that binds to the P2VP blocks was added to the gold-loaded polymer solution and stirred for 12 h. Finally, the polymer solution was spin-coated onto a glass slide at 2000 rpm for 60 s. Metal nanoparticles were formed by using the reducing agent sodium borohydride (NaBH_4). While these films were used for optical measurements, we removed the polymer template by oxygen plasma treatment to perform SFM measurements of the Ag/Au composite nanoparticle array, as shown in Figure 2b.

In Figure 2c, we show the extinction spectrum of the Au/Ag nanoparticle array that displays two LSP resonances at 411 and 578 nm. The double peak spectrum is a clear indication that the Au/Ag particles in the array are composite nanostructures made of distinct Au and Ag subunits. Alloyed Au/Ag nanoparticles would display a single LSP resonance with a resonance

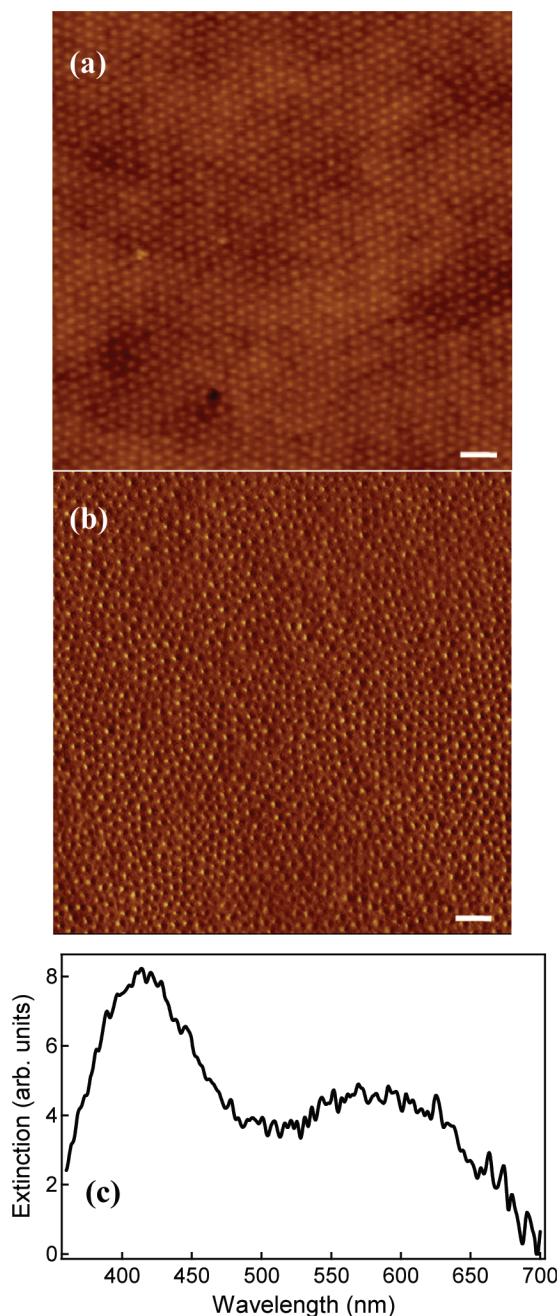


Figure 2. SFM images of the spin-coated PS-*b*-P2VP/PS-*b*-PEO blend system (a) and the Au/Ag composite nanoparticle array prepared from this BCP template (b). Scale bars are 100 nm. (c) Extinction spectrum of the Au/Ag composite nanoparticle array, displaying two distinct LSP resonances.

wavelength that is tunable between the Ag and Au resonances (~ 400 – 530 nm range) depending on the Au/Ag ratio.²² Extinction measurements of Ag/Au nanoparticle arrays after oxygen treatment (as used to remove the polymer template) did not show any resonance in the 400 nm region, indicating that the silver oxidized. These nanoarrays with double LSP resonances in the visible wavelength range can be very attractive as substrates that increase the sensitivity of fluorescence sensors. When the short wavelength LSP resonance is tuned to the absorption band and the long

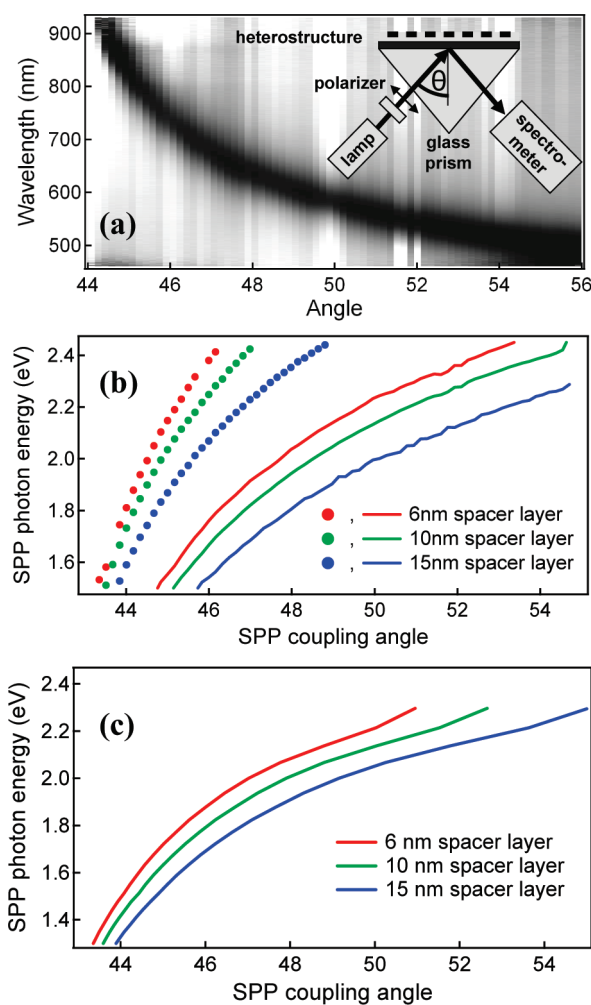


Figure 3. (a) Reflectivity plot of the Au/Ag composite nanoparticle thin film structure with a 15 nm silicon oxide spacer layer. Inset: Schematic of the experimental configuration. Measured (b) and calculated (c) SPP photon energy as a function of SPP coupling angle for spacer layers with thicknesses 6 nm (red), 10 nm (green), and 15 nm (blue). The dotted lines in (b) are measured data from the reference samples that consist of silver films and dielectric spacer layers, but without gold nanoparticle arrays.

wavelength LSP resonance to the emission of a fluorophore, both absorption and emission can get enhanced,^{23–26} thereby increasing the fluorescence and the sensor's sensitivity significantly. It has to be noted that efficient emission enhancement would require larger nanoparticles than the ones produced in this work.²⁴

As an example of the flexibility of the patterning process for producing functional plasmonic nanostructures, we deposited BCP-based gold nanoarrays onto silver thin films to study the interaction between LSPs and SPPs that propagate on extended metal surfaces. Structures that combine metal films and nanoparticles with appropriate dimensions are expected to produce strong electric field enhancements in the gap between the metal nanoparticles and the metal film²⁷ and, therefore, are attractive for functional components in plasmonic circuits that re-

quire strong non-linearities. Our hybrid LSP/SPP samples consist of ~ 50 nm thick silver films deposited by electron beam evaporation and BCP gold nanoparticle arrays. Silicon oxide layers with different thicknesses were evaporated onto the silver films before BCP patterning to serve as dielectric spacer layers that control the interaction between the LSPs of the gold nanoparticles and the SPPs of the thin silver film. We then mounted the samples onto a prism and measured the reflectivity of a collimated, p-polarized white light beam from the back of the sample in the Kretschmann–Raether prism configuration (inset of Figure 3a). Such a configuration is the standard way to measure the dispersion relation of the SPP since the SPP manifests itself as an angle (momentum) and spectral (energy)-dependent minima in the reflectivity.²⁸ In the prism configuration, the resonance condition for the coupling between photons and SPPs at a metal/dielectric interface with dielectric functions ϵ_m and ϵ_d , respectively, is

$$k_{\text{SPP}} = \frac{2\pi}{\lambda} n_{\text{prism}} \sin(\theta_{\text{SPP}}) = \frac{2\pi}{\lambda} \sqrt{\frac{\epsilon_d \epsilon_m}{\epsilon_d + \epsilon_m}} \quad (2)$$

in which n_{prism} is the refractive index of the prism and θ_{SPP} is the coupling angle (see inset of Figure 3a).

In Figure 3a, we show a typical reflectivity map of a hybrid Au nanoparticle/Ag film structure that displays an angle- and wavelength-dependent dip in the reflectivity indicating the SPP coupling angle. From such plots, we extract the angle-resolved SPP coupling wavelength and display it in a dispersion-type plot in Figure 3b. We determined dispersion relations for Au nanoparticle/Ag film samples with dielectric spacer layers of 6, 10, and 15 nm thickness. As a control, we performed the same measurements and analysis with the Ag film samples only, in the absence of the Au nanoparticle array (Figure 3b). We find a clear difference between the hybrid and the control samples. For the same photon energy, the SPPs in the hybrid samples are excited at larger angles that correspond to larger wave vectors according to eq 2. Moreover, increasing the spacer layer thickness leads to larger coupling angles and wave vectors. Such behavior can be understood with an increase of the effective dielectric constant by the dielectric spacer layer and the Au nanoarray on top of the silver film. Increased wave vectors indicate slower propagation velocity and, therefore, stronger field concentrations that are advantageous for many plasmonic devices that require large field enhancements. It is noteworthy that the spectral width of the reflectivity dip does not differ significantly between Ag film samples with and without Au nanoparticles. Since the reflectivity dip width is a measure of the SPP damping, we conclude that the Au nano-

particles do not cause significant additional scattering losses.

To test our explanation, we calculated the optical response of the hybrid Au nanoarray/Ag thin film samples using a transfer matrix formalism for multilayer systems. The Au nanoparticle array layer is modeled as a layer of thickness 15 nm with oblate nanoparticles that occupy a volume fraction p (equal the area density of the nanoarray) inside a matrix with dielectric constant ϵ_d . The effective dielectric function ϵ_{eff} of this layer is then given by

$$\epsilon_{\text{eff}} = \epsilon_d \frac{\epsilon_d + L(\epsilon_m - \epsilon_d) + p(1 - L)(\epsilon_m - \epsilon_d)}{\epsilon_d + L(\epsilon_m - \epsilon_d) - pL(\epsilon_m - \epsilon_d)} \quad (3)$$

Here, we consider the LSP resonance with electric field along the *short* axis of the Au ellipsoids ($L = 0.41$) because the electrical field component of the SPP perpendicular to the surface is stronger than the parallel one. In Figure 3c, we show the calculated SPP resonance photon energy as a function of excitation angles for the same dielectric spacer layers as in the experiment. The correspondence between calculated and measured SPP dispersion relations is very good, supporting the applied model and the notion that the gold nanoparticle array is the reason for the increased SPP wave vector. It has to be noted here that the inter-

action between LSP and SPPs is in the weak coupling regime, primarily because of the small dimensions of the nanoparticles. Strong coupling would lead to a distinct distortion of the SPP dispersion relation at the LSP resonance frequency.²⁹ Such an effect is not observed in our measurements but is the subject of further studies with larger nanoparticles that have larger scattering cross sections.

CONCLUSIONS

In conclusion, we have successfully manufactured dense and ordered arrays of metal nanostructures by reducing metal salts in BCP templates. Besides single-component nanoparticle arrays that exhibit a single LSP resonance, we fabricated composite nanoparticle arrays that display two characteristic LSP resonances. Applied onto a plane silver film, our gold nanoparticle arrays led to a substantial increase of the SPP wave vector, indicating localization of electromagnetic energy densities. Hence, these metal nanoarrays are promising plasmonic components for enhancing electric fields either in a stand alone configuration or in conjunction with metallic substrates. Macroscopic patterning (*e.g.*, to form nanoparticle wires) should be possible by electron beam writing onto the BCP templates.³⁰ Moreover, dense gold nanoparticle arrays can be attractive seed substrates for producing high density nanowire arrays by vapor–liquid–solid (VLS) deposition techniques.³¹

EXPERIMENTAL DETAILS

Au Nanoparticle Arrays: BCP films were prepared by spin-coating 0.5 wt % PS-*b*-P4VP copolymer toluene/tetrahydrofuran (THF) (70/30, v/v) solutions onto glass coverslips. The copolymer purchased from Polymer Source has a molecular weight of 68.7 kg/mol ($M_n^{\text{PS}} = 47.6$ kg/mol; $M_n^{\text{P4VP}} = 20.9$ kg/mol) and a polydispersity (M_w/M_n) of 1.14. After solvent annealing in THF, the films were immersed in a gold salt solution (HAuCl₄, 1 wt %) for 5 min to complex gold ions to 4-vinylpyridine units, followed by rinsing several times with pure water.

Au/Ag Nanoparticle Arrays: The 0.5 wt % PS-*b*-P2VP/PS-*b*-PEO (50/50, w/w) copolymer blends were used to produce the BCP templates by spin-coating without additional annealing. The PS-*b*-PEO ($M_n = 43.0$ kg/mol, $M_w/M_n = 1.06$, and the weight percent of PS = 69%) and PS-*b*-P2VP ($M_n = 58.0$ kg/mol, $M_w/M_n = 1.07$, and the weight percent of PS = 74.4%) were purchased from Polymer Source.

Optical Experiments: Extinction measurements were performed with a tungsten halogen lamp from Avantes (AvaLight-HAL), an Acton series spectrograph (SP2300), and a thermoelectric cooled CCD camera (PIXIS 100B) from Princeton Instruments. For measuring the angle and spectrally resolved reflectivity of the hybrid Au nanoarray/Ag film samples, we used the same tungsten halogen lamp, motorized rotation stages from Newport Corporation (PR50PP), and a spectrometer from Ocean Optics (USB4000).

Acknowledgment. The authors would like to acknowledge financial support from the National Science Foundation under Grant ECCS-0725609 and the MRSEC program and the U.S. Department of Energy Office of Basic Energy Science. S.P. was supported by the WCU Program (R31-2008-000-20012-0) through the NRF.

REFERENCES AND NOTES

- Veselago, V. G. Electrodynamics of Substances with Simultaneously Negative Values of Sigma and Mu. *Sov. Phys. Usp.* **1968**, *10*, 509–514.
- Pendry, J. B. Negative Refraction Makes a Perfect Lens. *Phys. Rev. Lett.* **2000**, *85*, 3966–3969.
- Elser, J.; Wangberg, R.; Podolskiy, V. A.; Narimanov, E. E. Nanowire Metamaterials with Extreme Optical Anisotropy. *Appl. Phys. Lett.* **2006**, *89*, 261102.
- Barnes, W. L.; Dereux, A.; Ebbesen, T. W. Surface Plasmon Subwavelength Optics. *Nature* **2003**, *424*, 824–830.
- Henzie, J.; Lee, J.; Lee, M. H.; Hasan, W.; Odum, T. W. Nanofabrication of Plasmonic Structures. *Annu. Rev. Phys. Chem.* **2009**, *60*, 147–165.
- Haynes, C. L.; Van Duyne, R. P. Nanosphere Lithography: A Versatile Nanofabrication Tool for Studies of Size-Dependent Nanoparticle Optics. *J. Phys. Chem. B* **2001**, *105*, 5599–5611.
- Bigioni, T. P.; Lin, X. M.; Nguyen, T. T.; Corwin, E. I.; Witten, T. A.; Jaeger, H. M. Kinetically Driven Self Assembly of Highly Ordered Nanoparticle Monolayers. *Nat. Mater.* **2006**, *5*, 265–270.
- Cheng, W. L.; Campolongo, M. J.; Cha, J. J.; Tan, S. J.; Umbach, C. C.; Muller, D. A.; Luo, D. Free-Standing Nanoparticle Superlattice Sheets Controlled by DNA. *Nat. Mater.* **2009**, *8*, 519–525.
- Park, S.; Wang, J. Y.; Kim, B.; Russell, T. P. From Nanorings to Nanodots by Patterning with Block Copolymers. *Nano Lett.* **2008**, *8*, 1667–1672.
- Park, S.; Kim, B.; Wang, J. Y.; Russell, T. P. Fabrication of Highly Ordered Silicon Oxide Dots and Stripes from Block Copolymer Thin Films. *Adv. Mater.* **2008**, *20*, 681–685.
- Aizawa, M.; Buriak, J. M. Block Copolymer Templated Chemistry for the Formation of Metallic Nanoparticle

- Arrays on Semiconductor Surfaces. *Chem. Mater.* **2007**, *19*, 5090–5101.
12. Lohmueller, T.; Bock, E.; Spatz, J. P. Synthesis of Quasi-Hexagonal Ordered Arrays of Metallic Nanoparticles with Tunable Particle Size. *Adv. Mater.* **2008**, *20*, 2297–2302.
 13. Spatz, J. P.; Roescher, A.; Moller, M. Gold Nanoparticles in Micellar Poly(styrene)-*b*-Poly(ethylene oxide) Films—Size and Interparticle Distance Control in Monoparticulate Films. *Adv. Mater.* **1996**, *8*, 337–340.
 14. Zhang, J. G.; Gao, Y.; Alvarez-Puebla, R. A.; Buriak, J. M.; Fenniri, H. Synthesis and SERS Properties of Nanocrystalline Gold Octahedra Generated from Thermal Decomposition of H₂AuCl₄ in Block Copolymers. *Adv. Mater.* **2006**, *18*, 3233–3237.
 15. Goy-Lopez, S.; Castro, E.; Taboada, P.; Mosquera, V. Block Copolymer-Mediated Synthesis of Size-Tunable Gold Nanospheres and Nanoplates. *Langmuir* **2008**, *24*, 13186–13196.
 16. Lu, J.; Chamberlin, D.; Rider, D. A.; Liu, M. Z.; Manners, I.; Russell, T. P. Using a Ferrocenylsilane-Based Block Copolymer as a Template to Produce Nanotextured Ag Surfaces: Uniformly Enhanced Surface Enhanced Raman Scattering Active Substrates. *Nanotechnology* **2006**, *17*, 5792–5797.
 17. Wang, Y.; Becker, M.; Wang, L.; Liu, J. Q.; Scholz, R.; Peng, J.; Gosele, U.; Christiansen, S.; Kim, D. H.; Steinhart, M. Nanostructured Gold Films for SERS by Block Copolymer-Templated Galvanic Displacement Reactions. *Nano Lett.* **2009**, *9*, 2384–2389.
 18. Romero, I.; Aizpurua, J.; Bryant, G. W.; de Abajo, F. J. G. Plasmons in Nearly Touching Metallic Nanoparticles: Singular Response in the Limit of Touching Dimers. *Opt. Express* **2006**, *14*, 9988–9999.
 19. Van de Hulst, H. C. *Light Scattering by Small Particles*; Wiley: New York, 1957.
 20. Johnson, P. B.; Christy, R. W. Optical-Constants of Noble-Metals. *Phys. Rev. B* **1972**, *6*, 4370–4379.
 21. Jeon, S. M.; Jang, K. Y.; Lee, S. H.; Park, H. W.; Sohn, B. H. Synthesis of Atypical Nanoparticles by the Nanostructure in Thin Films of Triblock Copolymers. *Langmuir* **2008**, *24*, 11137–11140.
 22. Sinzig, J.; Radtke, U.; Quinten, M.; Kreibitz, U. Binary Clusters—Homogeneous Alloys and Nucleus-Shell Structures. *Z. Phys. D: At., Mol. Clusters* **1993**, *26*, 242–245.
 23. Kuhn, S.; Hakanson, U.; Rogobete, L.; Sandoghdar, V. Enhancement of Single-Molecule Fluorescence Using a Gold Nanoparticle as an Optical Nanoantenna. *Phys. Rev. Lett.* **2006**, *97*, 017402.
 24. Anger, P.; Bharadwaj, P.; Novotny, L. Enhancement and Quenching of Single-Molecule Fluorescence. *Phys. Rev. Lett.* **2006**, *96*, 113002.
 25. Tam, F.; Goodrich, G. P.; Johnson, B. R.; Halas, N. J. Plasmonic Enhancement of Molecular Fluorescence. *Nano Lett.* **2007**, *7*, 496–501.
 26. Wang, Y.; Yang, T.; Tuominen, M.; Achermann, M. Radiative Rate Enhancements in Hybrid Metal-Semiconductor Nanostructures. *Phys. Rev. Lett.* **2009**, *102*, 163001.
 27. Leveque, G.; Martin, O. J. F. Tunable Composite Nanoparticle for Plasmonics. *Opt. Lett.* **2006**, *31*, 2750–2752.
 28. Yalcin, S. E.; Wang, Y.; Achermann, M. Spectral Bandwidth and Phase Effects of Resonantly Excited Ultrafast Surface Plasmon Pulses. *Appl. Phys. Lett.* **2008**, *93*, 101103.
 29. Chu, Y. Z.; Crozier, K. B. Experimental Study of the Interaction between Localized and Propagating Surface Plasmons. *Opt. Lett.* **2009**, *34*, 244–246.
 30. Park, S.; Yavuzcetin, O.; Kim, B.; Tuominen, M. T.; Russell, T. P. A Simple Top-Down/Bottom-Up Approach to Sectorized, Ordered Arrays of Nanoscopic Elements Using Block Copolymers. *Small* **2009**, *5*, 1064–1069.
 31. Wagner, R. S.; Ellis, W. C. Vapor–Liquid–Solid Mechanism of Single Crystal Growth. *Appl. Phys. Lett.* **1964**, *4*, 89–91.